EUROPEAN ORGANIZATION FOR NUCLEAR RESEARCH

CERN–PPE/94-219

20 December 1994

First Measurement of the Strange Quark Asymmetry at the Z^0 Peak

DELPHI Collaboration

Abstract

A measurement of the strange quark forward–backward asymmetry at the Z^0 peak was performed using 718,000 multihadronic Z^0 decays collected by the DELPHI detector at LEP in 1992. The $s-$quark was tagged by the presence of high momentum charged kaons identified by the Ring Imaging Cherenkov detector and by Λ^0's decaying into $p\pi^-$. The $s-$quark purity obtained was estimated for the two hadrons to be 43%. The average $s-$quark asymmetry was found to be $0.131 \pm 0.035\ (stat.) \pm 0.013\ (syst.)$. The forward–backward asymmetry was measured for unresolved $d-$ and $s-$quarks, tagged by the detection of a high energy neutron or neutral kaon in the Hadron Calorimeter. The combined $d-$ and $s-$quark purity was 69% and their asymmetry was found to be $0.112 \pm 0.031\ (stat.) \pm 0.054\ (syst.)$.

(To be submitted to Physics Letters B)

P.Abreu[21], W.Adam[8], T.Adye[38], E.Agasi[31], I.Ajinenko[43], R.Aleksan[40], G.D.Alekseev[15], P.P.Allport[22], S.Almehed[24], F.M.L.Almeida[48], S.J.Alvsvaag[4], U.Amaldi[8], S.Amato[48], A.Andreazza[28], M.L.Andrieux[13], P.Antilogus[25], W-D.Apel[16], Y.Arnoud[40], B.Åsman[45], J-E.Augustin[19], A.Augustinus[31], P.Baillon[8], P.Bambade[19], F.Barao[21], R.Barate[13], D.Y.Bardin[15], G.J.Barker[35], A.Baroncelli[41], O.Barring[8], J.A.Barrio[26], W.Bartl[51], M.J.Bates[38], M.Battaglia[14], M.Baubillier[23], J.Baudot[40], K-H.Becks[53], M.Begalli[37], P.Beilliere[7], Yu.Belokopytov[8], P.Beltran[10], A.C.Benvenuti[5], M.Berggren[42], D.Bertrand[2], F.Bianchi[46], M.Bigi[46], M.S.Bilenky[15], P.Billoir[23], J.Bjarne[24], D.Bloch[9], M.Blume[53], S.Blyth[35], V.Bocci[39], T.Bolognese[40], M.Bonesini[28], W.Bonivento[28], P.S.L.Booth[22], G.Borisov[43], C.Bosio[41], B.Bostjancic[44], S.Bosworth[35], O.Botner[49], B.Bouquet[19], C.Bourdarios[19], T.J.V.Bowcock[22], M.Bozzo[12], P.Branchini[41], K.D.Brand[36], R.A.Brenner[14], H.Briand[23], C.Bricman[2], L.Brillault[23], R.C.A.Brown[8], P.Bruckman[17], J-M.Brunet[7], L.Bugge[33], T.Buran[33], A.Buys[8], M.Caccia[28], M.Calvi[28], A.J.Camacho Rozas[42], T.Camporesi[8], V.Canale[39], M.Canepa[12], K.Cankocak[45], F.Cao[2], F.Carena[8], P.Carrilho[48], L.Carroll[22], C.Caso[12], V.Cassio[46], M.V.Castillo Gimenez[50], A.Cattai[8], F.R.Cavallo[5], L.Cerrito[39], V.Chabaud[8], A.Chan[1], Ph.Charpentier[8], L.Chaussard[25], J.Chauveau[23], P.Checchia[36], G.A.Chelkov[15], P.Chliapnikov[43], P.Chochula[6], V.Chorowicz[8], J.T.M.Chrin[50], V.Cindro[44], P.Collins[8], J.L.Contreras[19], R.Contri[12], E.Cortina[50], G.Cosme[19], F.Cossutti[47], H.B.Crawley[1], D.Crennell[38], G.Crosetti[12], J.Cuevas Maestro[34], S.Czellar[14], E.Dahl-Jensen[29], J.Dahm[53], B.Dalmagne[19], M.Dam[33], G.Damgaard[29], A.Daum[16], P.D.Dauncey[38], M.Davenport[8], W.Da Silva[23], C.Defoix[7], G.Della Ricca[47], P.Delpierre[27], N.Demaria[35], A.De Angelis[8], H.De Boeck[2], W.De Boer[16], S.De Brabandere[2], C.De Clercq[2], M.D.M.De Fez Laso[50], C.De La Vaissiere[23], B.De Lotto[47], A.De Min[28], L.De Paula[48], C.De Saint-Jean[40], H.Dijkstra[8], L.Di Ciaccio[39], F.Djama[9], J.Dolbeau[7], M.Donszelmann[8], K.Doroba[52], M.Dracos[9], J.Drees[53], K.-A.Drees[53], M.Dris[32], Y.Dufour[7], F.Dupont[13], D.Edsall[1], R.Ehret[16], T.Ekelof[49], G.Ekspong[45], M.Elsing[53], J-P.Engel[9], N.Ershaidat[23], M.Espirito Santo[21], D.Fassouliotis[32], M.Feindt[8], A.Fenyuk[43], A.Ferrer[50], T.A.Filippas[32], A.Firestone[1], H.Foeth[8], E.Fokitis[32], F.Fontanelli[12], F.Formenti[8], J-L.Fousset[27], B.Franek[38], P.Frenkiel[7], D.C.Fries[16], A.G.Frodesen[4], R.Fruhwirth[51], F.Fulda-Quenzer[19], H.Furstenau[8], J.Fuster[8], D.Gamba[46], M.Gandelman[18], C.Garcia[50], J.Garcia[42], C.Gaspar[8], U.Gasparini[36], Ph.Gavillet[8], E.N.Gazis[32], D.Gele[9], J-P.Gerber[9], D.Gillespie[8], R.Gokieli[52], B.Golob[44], J.J.Gomez Y Cadenas[8], G.Gopal[38], L.Gorn[1], M.Gorski[52], V.Gracco[12], F.Grard[2], E.Graziani[41], G.Grosdidier[19], P.Gunnarsson[45], J.Guy[38], U.Haedinger[16], F.Hahn[53], M.Hahn[16], S.Hahn[53], S.Haider[31], Z.Hajduk[17], A.Hakansson[24], A.Hallgren[49], K.Hamacher[53], W.Hao[31], F.J.Harris[35], V.Hedberg[24], R.Henriques[21], J.J.Hernandez[50], J.A.Hernando[50], P.Herquet[2], H.Herr[8], T.L.Hessing[8], E.Higon[50], H.J.Hilke[8], T.S.Hill[1], S-O.Holmgren[45], P.J.Holt[35], D.Holthuizen[31], P.F.Honore[7], M.Houlden[22], K.Huet[2], K.Hultqvist[45], P.Ioannou[3], J.N.Jackson[22], R.Jacobsson[45], P.Jalocha[17], R.Janik[6], G.Jarlskog[24], P.Jarry[40], B.Jean-Marie[19], E.K.Johansson[45], L.Jonsson[24], P.Juillot[9], M.Kaiser[16], G.Kalmus[38], F.Kapusta[23], M.Karlsson[45], E.Karvelas[10], S.Katsanevas[3], E.C.Katsoufis[32], R.Keranen[14], B.A.Khomenko[15], N.N.Khovanski[15], B.King[22], N.J.Kjaer[29], H.Klein[8], A.Klovning[4], P.Kluit[31], J.H.Koehne[16], B.Koene[31], P.Kokkinias[10], M.Koratzinos[8], K.Korcyl[17], V.Kostioukhine[43], C.Kourkoumelis[3], O.Kouznetsov[12], P.-H.Kramer[53], M.Krammer[51], C.Kreuter[16], J.Krolikowski[52], I.Kronkvist[24], Z.Krumstein[15], W.Krupinski[17], P.Kubinec[6], W.Kucewicz[17], K.Kulka[49], K.Kurvinen[14], C.Lacasta[50], I.Laktineh[25], C.Lambropoulos[10], J.W.Lamsa[1], L.Lanceri[47], D.W.Lane[1], P.Langefeld[53], V.Lapin[43], I.Last[22], J-P.Laugier[40], R.Lauhakangas[14], G.Leder[51], F.Ledroit[13], V.Lefebure[2], C.K.Legan[1], R.Leitner[30], Y.Lemoigne[40], J.Lemonne[2], G.Lenzen[53], V.Lepeltier[19], T.Lesiak[36], D.Liko[51], A.Lilja[14], R.Lindner[53], A.Lipniacka[19], I.Lippi[36], B.Loerstad[24], M.Lokajicek[11], J.G.Loken[35], A.Lopez-Fernandez[8], M.A.Lopez Aguera[42], D.Loukas[10], J.J.Lozano[50], P.Lutz[40], L.Lyons[35], G.Maehlum[16], J.Maillard[7], A.Maio[21], A.Maltezos[10], V.Malychev[15], F.Mandl[51], J.Marco[42], B.Marechal[48], M.Margoni[36], J-C.Marin[8], C.Mariotti[41], A.Markou[10], T.Maron[53], C.Martinez-Rivero[42], F.Martinez-Vidal[50], S.Marti i Garcia[50], F.Matorras[42], C.Matteuzzi[28], G.Matthiae[39], M.Mazzucato[36], M.Mc Cubbin[8], R.Mc Kay[1], R.Mc Nulty[22], J.Medbo[49], C.Meroni[28], W.T.Meyer[1], M.Michelotto[36], E.Migliore[46], I.Mikulec[51], L.Mirabito[25], W.A.Mitaroff[51], U.Mjoernmark[24], T.Moa[45], R.Moeller[29], K.Moenig[8], M.R.Monge[12], P.Morettini[12], H.Mueller[16], W.J.Murray[38], B.Muryn[17], G.Myatt[35], F.Naraghi[13], F.L.Navarria[5], S.Navas[50], P.Negri[28], S.Nemecek[11], W.Neumann[53], N.Neumeister[51], R.Nicolaidou[3], B.S.Nielsen[29], V.Nikolaenko[25], P.Niss[45], A.Nomerotski[36], A.Normand[35], W.Oberschulte-Beckmann[16], V.Obraztsov[43], A.G.Olshevski[15], R.Orava[14], K.Osterberg[14], A.Ouraou[40], P.Paganini[19], M.Paganoni[28], P.Pages[9], R.Pain[23], H.Palka[17], Th.D.Papadopoulou[32], L.Pape[8], F.Parodi[12], A.Passeri[41], M.Pegoraro[36], J.Pennanen[14], L.Peralta[21], V.Perevozchikov[43], H.Pernegger[51], M.Pernicka[51], A.Perrotta[5], C.Petridou[47], A.Petrolini[12], H.T.Phillips[38], G.Piana[12], F.Pierre[40], M.Pimenta[21], S.Plaszczynski[19], O.Podobrin[16], M.E.Pol[18], G.Polok[17], P.Poropat[47], V.Pozdniakov[15], M.Prest[47], P.Privitera[39], A.Pullia[28], D.Radojicic[35], S.Ragazzi[28], H.Rahmani[32], J.Rames[11], P.N.Ratoff[20], A.L.Read[33], M.Reale[53], P.Rebecchi[19], N.G.Redaelli[28], M.Regler[51], D.Reid[8], P.B.Renton[35], L.K.Resvanis[3], F.Richard[19], J.Richardson[22], J.Ridky[11], G.Rinaudo[46], I.Ripp[40], A.Romero[46], I.Roncagliolo[12], P.Ronchese[36], L.Roos[13], E.I.Rosenberg[1], E.Rosso[8], P.Roudeau[19], T.Rovelli[5], W.Ruckstuhl[31], V.Ruhlmann-Kleider[40], A.Ruiz[42], A.Rybin[43], H.Saarikko[14], Y.Sacquin[40], A.Sadovsky[15], G.Sajot[13], J.Salt[50], J.Sanchez[26], M.Sannino[12], H.Schneider[16], M.A.E.Schyns[53], G.Sciolla[46], F.Scuri[47], Y.Sedykh[15], A.M.Segar[35], A.Seitz[16], R.Sekulin[38], R.C.Shellard[37], I.Siccama[31], P.Siegrist[40], S.Simonetti[40], F.Simonetto[36], A.N.Sisakian[15], B.Sitar[6], T.B.Skaali[33], G.Smadja[25], N.Smirnov[43], O.Smirnova[15], G.R.Smith[38], R.Sosnowski[52], D.Souza-Santos[37], T.Spassov[21], E.Spiriti[41], S.Squarcia[12], H.Staeck[53], C.Stanescu[41], S.Stapnes[33], I.Stavitski[36], G.Stavropoulos[10], K.Stepaniak[52], F.Stichelbaut[8], A.Stocchi[19], J.Strauss[51], R.Strub[9], B.Stugu[4],

M.Szczekowski[52], M.Szeptycka[52], T.Tabarelli[28], O.Tchikilev[43], G.E.Theodosiou[10], A.Tilquin[27], J.Timmermans[31], L.G.Tkatchev[15], T.Todorov[9], D.Z.Toet[31], A.Tomaradze[2], B.Tome[21], E.Torassa[46], L.Tortora[41], G.Transtromer[24], D.Treille[8], W.Trischuk[8], G.Tristram[7], A.Trombini[19], C.Troncon[28], A.Tsirou[8], M-L.Turluer[40], I.A.Tyapkin[23], M.Tyndel[38], S.Tzamarias[22], B.Ueberschaer[53], S.Ueberschaer[53], O.Ullaland[8], V.Uvarov[43], G.Valenti[5], E.Vallazza[8], J.A.Valls Ferrer[50], G.W.Van Apeldoorn[31], P.Van Dam[31], W.K.Van Doninck[2], J.Van Eldik[31], G.Vegni[28], L.Ventura[36], W.Venus[38], F.Verbeure[2], M.Verlato[36], L.S.Vertogradov[15], D.Vilanova[40], P.Vincent[25], L.Vitale[47], E.Vlasov[43], A.S.Vodopyanov[15], M.Voutilainen[14], V.Vrba[11], H.Wahlen[53], C.Walck[45], F.Waldner[47], A.Wehr[53], M.Weierstall[53], P.Weilhammer[8], A.M.Wetherell[8], D.Wicke[53], J.H.Wickens[2], M.Wielers[16], G.R.Wilkinson[35], W.S.C.Williams[35], M.Winter[9], M.Witek[8], G.Wormser[19], K.Woschnagg[49], K.Yip[35], L.Yu[35], O.Yushchenko[43], F.Zach[25], A.Zaitsev[43], A.Zalewska[17], P.Zalewski[52], D.Zavrtanik[44], E.Zevgolatakos[10], N.I.Zimin[15], M.Zito[40], D.Zontar[44], R.Zuberi[35], G.C.Zucchelli[45], G.Zumerle[36]

[1] Ames Laboratory and Department of Physics, Iowa State University, Ames IA 50011, USA
[2] Physics Department, Univ. Instelling Antwerpen, Universiteitsplein 1, B-2610 Wilrijk, Belgium
and IIHE, ULB-VUB, Pleinlaan 2, B-1050 Brussels, Belgium
and Faculté des Sciences, Univ. de l'Etat Mons, Av. Maistriau 19, B-7000 Mons, Belgium
[3] Physics Laboratory, University of Athens, Solonos Str. 104, GR-10680 Athens, Greece
[4] Department of Physics, University of Bergen, Allégaten 55, N-5007 Bergen, Norway
[5] Dipartimento di Fisica, Università di Bologna and INFN, Via Irnerio 46, I-40126 Bologna, Italy
[6] Comenius University, Faculty of Mathematics and Physics, Mlynska Dolina, SK-84215 Bratislava, Slovakia
[7] Collège de France, Lab. de Physique Corpusculaire, IN2P3-CNRS, F-75231 Paris Cedex 05, France
[8] CERN, CH-1211 Geneva 23, Switzerland
[9] Centre de Recherche Nucléaire, IN2P3 - CNRS/ULP - BP20, F-67037 Strasbourg Cedex, France
[10] Institute of Nuclear Physics, N.C.S.R. Demokritos, P.O. Box 60228, GR-15310 Athens, Greece
[11] FZU, Inst. of Physics of the C.A.S. High Energy Physics Division, Na Slovance 2, 180 40, Praha 8, Czech Republic
[12] Dipartimento di Fisica, Università di Genova and INFN, Via Dodecaneso 33, I-16146 Genova, Italy
[13] Institut des Sciences Nucléaires, IN2P3-CNRS, Université de Grenoble 1, F-38026 Grenoble Cedex, France
[14] Research Institute for High Energy Physics, SEFT, P.O. Box 9, FIN-00014 Helsinki, Finland
[15] Joint Institute for Nuclear Research, Dubna, Head Post Office, P.O. Box 79, 101 000 Moscow, Russian Federation
[16] Institut für Experimentelle Kernphysik, Universität Karlsruhe, Postfach 6980, D-76128 Karlsruhe, Germany
[17] High Energy Physics Laboratory, Institute of Nuclear Physics, Ul. Kawiory 26a, PL-30055 Krakow 30, Poland
[18] Centro Brasileiro de Pesquisas Físicas, rua Xavier Sigaud 150, BR-22290 Rio de Janeiro, Brazil
[19] Université de Paris-Sud, Lab. de l'Accélérateur Linéaire, IN2P3-CNRS, Bat 200, F-91405 Orsay Cedex, France
[20] School of Physics and Materials, University of Lancaster, Lancaster LA1 4YB, UK
[21] LIP, IST, FCUL - Av. Elias Garcia, 14-1^{o}, P-1000 Lisboa Codex, Portugal
[22] Department of Physics, University of Liverpool, P.O. Box 147, Liverpool L69 3BX, UK
[23] LPNHE, IN2P3-CNRS, Universités Paris VI et VII, Tour 33 (RdC), 4 place Jussieu, F-75252 Paris Cedex 05, France
[24] Department of Physics, University of Lund, Sölvegatan 14, S-22363 Lund, Sweden
[25] Université Claude Bernard de Lyon, IPNL, IN2P3-CNRS, F-69622 Villeurbanne Cedex, France
[26] Universidad Complutense, Avda. Complutense s/n, E-28040 Madrid, Spain
[27] Univ. d'Aix - Marseille II - CPP, IN2P3-CNRS, F-13288 Marseille Cedex 09, France
[28] Dipartimento di Fisica, Università di Milano and INFN, Via Celoria 16, I-20133 Milan, Italy
[29] Niels Bohr Institute, Blegdamsvej 17, DK-2100 Copenhagen 0, Denmark
[30] NC, Nuclear Centre of MFF, Charles University, Areal MFF, V Holesovickach 2, 180 00, Praha 8, Czech Republic
[31] NIKHEF-H, Postbus 41882, NL-1009 DB Amsterdam, The Netherlands
[32] National Technical University, Physics Department, Zografou Campus, GR-15773 Athens, Greece
[33] Physics Department, University of Oslo, Blindern, N-1000 Oslo 3, Norway
[34] Dpto. Fisica, Univ. Oviedo, C/P. Pérez Casas, S/N-33006 Oviedo, Spain
[35] Department of Physics, University of Oxford, Keble Road, Oxford OX1 3RH, UK
[36] Dipartimento di Fisica, Università di Padova and INFN, Via Marzolo 8, I-35131 Padua, Italy
[37] Depto. de Fisica, Pontificia Univ. Católica, C.P. 38071 RJ-22453 Rio de Janeiro, Brazil
[38] Rutherford Appleton Laboratory, Chilton, Didcot OX11 OQX, UK
[39] Dipartimento di Fisica, Università di Roma II and INFN, Tor Vergata, I-00173 Rome, Italy
[40] Centre d'Etude de Saclay, DSM/DAPNIA, F-91191 Gif-sur-Yvette Cedex, France
[41] Istituto Superiore di Sanità, Ist. Naz. di Fisica Nucl. (INFN), Viale Regina Elena 299, I-00161 Rome, Italy
[42] C.E.A.F.M., C.S.I.C. - Univ. Cantabria, Avda. los Castros, S/N-39006 Santander, Spain, (CICYT-AEN93-0832)
[43] Inst. for High Energy Physics, Serpukov P.O. Box 35, Protvino, (Moscow Region), Russian Federation
[44] J. Stefan Institute and Department of Physics, University of Ljubljana, Jamova 39, SI-61000 Ljubljana, Slovenia
[45] Fysikum, Stockholm University, Box 6730, S-113 85 Stockholm, Sweden
[46] Dipartimento di Fisica Sperimentale, Università di Torino and INFN, Via P. Giuria 1, I-10125 Turin, Italy
[47] Dipartimento di Fisica, Università di Trieste and INFN, Via A. Valerio 2, I-34127 Trieste, Italy
and Istituto di Fisica, Università di Udine, I-33100 Udine, Italy
[48] Univ. Federal do Rio de Janeiro, C.P. 68528 Cidade Univ., Ilha do Fundão BR-21945-970 Rio de Janeiro, Brazil
[49] Department of Radiation Sciences, University of Uppsala, P.O. Box 535, S-751 21 Uppsala, Sweden
[50] IFIC, Valencia-CSIC, and D.F.A.M.N., U. de Valencia, Avda. Dr. Moliner 50, E-46100 Burjassot (Valencia), Spain
[51] Institut für Hochenergiephysik, Österr. Akad. d. Wissensch., Nikolsdorfergasse 18, A-1050 Vienna, Austria
[52] Inst. Nuclear Studies and University of Warsaw, Ul. Hoza 69, PL-00681 Warsaw, Poland
[53] Fachbereich Physik, University of Wuppertal, Postfach 100 127, D-42097 Wuppertal 1, Germany

1 Introduction

The Standard Model of electroweak interactions predicts a forward–backward asymmetry in e^+e^- collisions near the Z^0 peak. The differential e^+e^- cross–section into a fermion pair $f\bar{f}$ can be expressed in the Born approximation as :

$$\frac{d\sigma_f}{d\cos\theta} = \sigma_f^{TOT}(s)\cdot\left[\frac{3}{8}(1+\cos^2\theta)+A_{FB}^f(s)\cdot\cos\theta\right] \quad (1)$$

where σ_f^{TOT} is the total cross–section, θ the production angle of the fermion f with respect to the incident electron direction and s the total energy squared. The forward–backward asymmetry is defined as :

$$A_{FB}^f(s) = \frac{\sigma_F^f-\sigma_B^f}{\sigma_F^f+\sigma_B^f} \quad (2)$$

where σ_F^f and σ_B^f are the fermion cross–sections in the forward and backward hemispheres (θ below and above 90°) respectively. As a function of θ, the forward–backward asymmetry can be expressed by :

$$A_{FB}^f(\theta) = \frac{8}{3}A_{FB}^f\frac{\cos\theta}{1+\cos^2\theta}\ . \quad (3)$$

At the Z^0 resonance, including only the Z^0 exchange diagram, A_{FB}^f is given by :

$$A_{FB}^f(M_Z^2) = \frac{3}{4}\left(\frac{2v_e a_e}{v_e^2+a_e^2}\right)\cdot\left(\frac{2v_f a_f}{v_f^2+a_f^2}\right) \quad (4)$$

where v_f and a_f are the vector and axial vector couplings of the fermions :

$$v_f = I_3^f - 2\cdot Q_f\cdot\sin^2\theta_W, \qquad a_f = I_3^f \quad (5)$$

and Q_f and I_3^f denote the charge and weak isospin of the fermions and θ_W is the weak effective mixing angle. The indices e and f refer to the initial electron and final fermion.

Asymmetry measurements in the quark sector have been reported by LEP experiments at the Z^0 peak for b and c quark pairs [1], yielding :

$$\begin{aligned} A_{FB}^b &= 0.0915\pm0.0037 \\ A_{FB}^c &= 0.0675\pm0.0091\ . \end{aligned} \quad (6)$$

This paper presents the first measurement of the asymmetry of the s–quark at the Z^0 peak. Comparing this measurement with the $b-$quark asymmetry measurement given in equation (6) checks the universality of the coupling constants. The experimental procedure used here is based on the identification of fast charged kaons and on the reconstruction of fast Λ^0 baryons decaying into a $p\pi^-$ pair. The forward–backward asymmetries of these hadrons are measured. Simulation is used to calculate A_{FB}^s from the measured hadron asymmetries and to evaluate the systematic errors coming from the hadronization model parameters. A complementary method for unresolved $s-$ and $d-$quark asymmetry measurement based on neutral hadron (K_L^0, n) detection is also presented. Figure 1 presents the hadron momentum distribution predicted by the JETSET 7.3 Parton Shower model [2] (JETSET PS in the following) separately for the five flavours. In each case, the $s\bar{s}$ contribution is larger than that of the other flavours, which justifies the choice of these hadrons for the $s-$quark asymmetry measurement.

2 Detector description and event selection

A general description of the DELPHI detector can be found in reference [3]. Features of the apparatus relevant for the analysis of multi-hadronic final states (with emphasis on the detection of charged particles) are outlined in reference [4]. The analysis presented here relies on the information provided by the following detectors: the micro Vertex Detector (VD), the Inner Detector (ID), the Time Projection Chamber (TPC), the Outer Detector (OD), the Forward drift Chambers (FCA and FCB), the barrel Ring Imaging CHerenkov detector (RICH), and the Hadron Calorimeter (HCAL).

The VD consists of 3 cylindrical layers of silicon, at radii 6.3 cm, 9.0 cm and 11.0 cm. They measure $R\phi$ coordinates transverse to the beam over a length along the beam axis of 24 cm. The polar angle coverage of the VD is from 29° to 151°.

The ID is a cylindrical drift chamber (inner radius 12 cm and outer radius 22 cm) covering polar angles between 29° and 151°.

The TPC, the principal tracking device of DELPHI, is a cylinder of 30 cm inner radius, 122 cm outer radius and has a length of 2.7 m. Each end-cap is divided into 6 sector plates, each with 192 sense wires used for the particle identification. The energy loss per unit length of a charged particle (dE/dx) is measured by the sense wires as the 80% truncated mean of the amplitudes of the wire signals. A dE/dx measurement is considered to be significant if at least 30 wires contribute to the energy loss measurement.

The OD consists of 5 layers of drift cells at radii between 192 cm and 208 cm, covering polar angles between 43° and 137°.

The Barrel RICH [5] covers the polar angle between 48° and 132°. It identifies the charged particles by measuring the angle of emission of the Cherenkov light, and thus the velocity. The mass of the charged particle is then extracted by using the velocity information combined with the momentum measurement. In order to cover a large momentum range, the DELPHI Barrel RICH uses two different Cherenkov radiators, one liquid (C_6F_{14}) allowing a π/K separation from 0.8 GeV/c to 3 GeV/c (not used in this analysis) and one gaseous (C_5F_{12}) separating kaons from pions from 2.5 GeV/c to 20 GeV/c.

The hadron calorimeter HCAL is a sampling gas detector incorporated in the magnet yoke, the barrel part covering polar angles between 42.6° and 137.4°, and two end-caps between 11.2° and 48.5° and between 131.5° and 168.8°. It consists of 21 iron plates of 5 cm thickness each. Between the iron plates wire chambers operating at limited streamer mode are assembled. They record the ionization electrons produced by the charged particles created in nuclear collisions between hadrons and iron nuclei of the plates. From the collected ionization charge the energy of the incident hadron can be extracted. The HCAL angular granularity is $\Delta\phi = 3.75°$ and $\Delta\theta = 2.96°$ in the barrel and $\Delta\theta = 2.62°$ in the end-caps. The relative energy resolution is $120\%/\sqrt{E}$ (E given in GeV).

The tracking in the forward ($11° < \theta < 33°$) and backward ($147° < \theta < 169°$) regions is ensured by two pairs of drift chambers (FCA and FCB) in the end–caps.

The average momentum resolution for the charged particles in hadronic final states is in the range $\Delta p/p^2 \simeq 0.001$ to 0.01 $(\mathrm{GeV}/c)^{-1}$, depending on which detectors are included in the track fit.

For the hadronic event selection, charged particles were accepted if : their momentum was larger than 0.1 GeV/c; the measured track length in the TPC was greater than 25 cm; their polar angle was between 25° and 155° and the relative error on the measured momentum was smaller than 100%.

Hadronic events were selected by requiring the total energy of the charged particles in each hemisphere to exceed 3 GeV (assuming all charged particles to be pions), the total energy of the charged particles to exceed 15 GeV and that there be at least 5 charged particles with momenta above 0.2 GeV/c.

A total of 718,000 events satisfied these cuts. Events due to beam-gas scattering and to $\gamma\gamma$ interactions have been estimated to be less than 0.1%. Background from $\tau^+\tau^-$ events has been estimated to be less than 0.2%.

In the analysis using charged kaons, only a subsample of 450,000 events was used for which the information from the gas radiator of the Barrel RICH was available.

The biases in the analysis due to the detector and the selection criteria were studied using the full detector simulation program DELSIM [6]. Events were generated using the JETSET PS model with parameters tuned as in reference [7] and with $\sin^2\theta_W = 0.232$. The particles were followed through the detailed detector geometry and the simulated data processed by the same analysis program as the real data.

3 Analysis

The measurement of the $s-$quark asymmetry involved three different techniques.

1. The first analysis requires the presence of high momentum charged kaons to tag decays of the Z^0 into a $s\bar{s}$ pair. The charge and the direction of the kaon indicates the charge and the direction of the quark. The momentum range of kaons used to study the $s-$quark asymmetry was 10 GeV/c to 18 GeV/c ($0.22 < x_p < 0.39$, where $x_p = 2p/\sqrt{s}$ with $\sqrt{s}$ the centre-of-mass energy and p the particle momentum). The choice of the range retains sensitivity to the $s-$quark asymmetry whilst allowing particle identification to be performed with good efficiency by the gaseous RICH. Table 1 gives the charged kaon asymmetry and kaon fraction coming from the five quark flavours in the JETSET PS model for this momentum range. The expected charged kaon asymmetry is $A_{FB}^{K^\pm} = 0.041$ with $Z^0 \rightarrow s\bar{s}$ decays giving 43% of the charged kaons.

2. The second analysis uses high momentum Λ^0 and $\overline{\Lambda^0}$ baryons[†] to tag decays of the Z^0 into a $s\bar{s}$ pair. The baryon number of the Λ^0 is related to its origin from an s quark. For this study Λ^0's decaying into $p\pi$ in the momentum range $11.41 < p_{\Lambda^0} < 22.82$ GeV/c ($0.25 < x_p < 0.50$) are considered. For higher x_p the detector does not provide high enough Λ^0 acceptance. Table 1 gives the Λ^0 asymmetry and fraction coming from all flavours predicted by the JETSET PS model. The expected Λ^0 asymmetry is 0.072 with a primary $s-$quark giving 43% of all Λ^0's.

3. The third technique uses high energy K_L^0 or neutrons (with an energy larger than 15 GeV) detected by the hadron calorimeter as a signature of a Z^0 decay into $s\bar{s}$ or $d\bar{d}$ pair. The sign of the primary quark is given by the statistical correlation between the charges of the initial quark and the resulting jet. Since in this method the s and d flavour contributions are not resolved due to the neutron presence, the measured asymmetry is the weighted mean of s and d asymmetries. In order to provide pure $s-$quark asymmetry measurement, a correction for neutrons is needed. Due to the absence of experimental data about neutron

[†] In the following when Λ^0 is mentioned, it also includes $\overline{\Lambda^0}$ unless explicitly stated.

production at LEP energies, this correction was not applied. Table 1 shows the expected neutron and K^0_L asymmetries and their relative abundance as they are produced by the different quark flavours in the Z^0 decays. The expected hadron asymmetry is 0.018 while the fraction of K^0_L and neutrons coming from primary $s-$ and $d-$quarks is 69%.

3.1 High momentum charged kaons

The particle identification capability of DELPHI with the Ring Imaging Cherenkov (RICH) detector is used to tag fast charged kaons.

A sample of 450,000 hadronic Z^0 decays has RICH information from the gas radiator for high momentum particles ($p > 2.5$ GeV/c). Figure 2 shows the mean Cherenkov angle θ_c versus the momentum p of charged particles with p higher than 9 GeV/c (the kaon threshold for Cherenkov radiation emission is at 8 GeV/c). Kaon rings are very well separated from saturated Cherenkov rings (e, μ, π) up to 18 GeV/c in the whole Barrel Rich acceptance. This upper limit varies with the particle direction (θ) according to the Cherenkov angle resolution (better resolution when $\cos\theta$ increases).

The corresponding mass squared (m^2) distribution to figure 2 can be calculated using the relation :

$$m^2 = p^2(n^2 \cos^2\theta_c - 1) \tag{7}$$

where n is the refractive index of the C_5F_{12} gas radiator (1.001893). Figure 3 shows the calculated m^2 distribution for all particles with momentum between 10 GeV/c and 18 GeV/c. A clear peak is observed around the kaon mass squared corresponding, as described below, to 19730 ± 200 $K^{\pm}$. Only charged particles with associated hits in the Outer Detector (after the Barrel RICH with respect to the interaction point) were used in order to reject particles lost before the Barrel RICH or badly reconstructed.

To avoid problems with the evaluation of the purity and contamination in particle identification, the following statistical method has been used to estimate the number of charged kaons. For each particle and for a given momentum the m^2 distribution is Gaussian. The width of this Gaussian distribution depends on the particle momentum p and has a term proportional to $(m^2 + p^2)$ due to the chromatic error on the Cherenkov angle [8]. After convolution with the particle momentum distribution (supposed to have an exponential form) and integration over the selected momentum range, the resulting distribution is in first approximation a Breit–Wigner like distribution. A fit to the m^2 distribution with the sum of two Breit–Wigner distributions, one for the saturated Cherenkov rings (e, μ, π) and one for kaons, gives the number of charged kaons.

The number of particles under the kaon peak versus the momentum is obtained by considering the mass squared distribution for 8 momentum ranges (with a width of 1 GeV/c) each fitted with the sum of two Breit–Wigner distributions. The extracted distribution has been fitted by an exponential distribution and is shown on figure 4.

Since the two parts of the Barrel RICH, side A ($92° < \theta < 132°$) and side C ($48° < \theta < 88°$), were not operated under exactly the same conditions (the main difference coming from "tripping" chambers), the asymmetry is measured separately for sides A and C in order to avoid the introduction of extra corrections :

$$\begin{aligned} A_{FB}^{K^{\pm},A}(\cos\theta) &= \frac{N^A_{K^+}(\cos\theta) - N^A_{K^-}(\cos\theta)}{N^A_{K^+}(\cos\theta) + N^A_{K^-}(\cos\theta)}\,, \\ A_{FB}^{K^{\pm},C}(\cos\theta) &= \frac{N^C_{K^-}(\cos\theta) - N^C_{K^+}(\cos\theta)}{N^C_{K^-}(\cos\theta) + N^C_{K^+}(\cos\theta)}\,. \end{aligned} \tag{8}$$

Finally, the weighted mean value of the two asymmetries (sides A and C) for each selected θ range is taken. Efficiency evaluation is not necessary because all efficiency factors (coming from geometry, detector malfunctioning, particle identification) cancel in the ratios. A systematic error induced by the separation of the two parts A and C comes from the detector material in front of the RICH gas radiator which leads to a higher probability of hadronic interactions for K^- than for K^+. Using the full DELPHI simulation [6] a correction on the number of K^- as a function of θ (varying from 2% to 6%) was determined and applied to the data. When the weighted mean value of the asymmetries of the two sides is taken the effect of this correction cancels to first order.

The m^2 distribution is considered for 6 separate θ ranges defined according to the angular coverage of the Barrel RICH mirrors (one point per mirror). The asymmetry obtained as a function of $\cos\theta$ is shown on figure 5, where θ is given by the kaon direction (the systematic error coming from the difference between the kaon and primary quark directions is discussed in section 4). A fit of equation (3) to the distribution of figure 5 yields a value of the forward–backward asymmetry for charged kaons of :

$$A_{FB}^{K^\pm} = 0.048 \pm 0.011\ (stat.) \pm 0.002\ (syst.)$$

with a $\chi^2/NDF = 4.4/5$.

The systematic error contributions to the charged kaon asymmetry are summarized in table 2. The main contribution comes from the signal parametrization. It has been extracted by varying the number of extra terms of higher order to the Breit–Wigner formula (which is a first order approximation). The limits of the momentum range in which the asymmetry measurement has been performed have been varied by ± 1 GeV/c. The contribution coming from the difference of hadronic interactions between K^+ and K^- is weak due to the cancelation mentioned above. A cross–check has been done by fitting the asymmetry distributions of each side separately after material correction. The obtained values are : $A_{FB}^{K^\pm,A} = 0.044 \pm 0.017$ and $A_{FB}^{K^\pm,C} = 0.051 \pm 0.014$ which are compatible within the statistical errors.

3.2 High momentum Λ^0

The Λ^0 baryons are detected by their decay into pπ. Secondary vertices of the Λ^0 decay are well separated from the primary vertex of the Z^0 decay due to the long Λ^0 lifetime and Lorentz boost.

Candidate secondary decays, V^0's, are found by considering all oppositely–charged particle pairs in the event. The Λ^0 decay vertex candidates were required to satisfy the following criteria:

- the radial separation of the primary and secondary vertex in the $R\phi$ plane must be greater than 10 times its error;
- in the $R\phi$ plane, the angle between the vector sum of the charged particle momenta and the line joining the primary to the secondary vertex must be less than $(10 + 20/p_t(V^0))$ mrad, where $p_t(V^0)$ is the transverse momentum of the V^0 relative to the beam axis (in GeV/c);
- when the radius at the reconstructed decay point of the V^0 is larger than the radius of the outer VD layer, the two particles must not have any associated hit in the VD;
- the χ^2 probability of the fitted secondary vertex must be larger than 0.001 to reject fake vertices;
- when the RICH information is available, the candidate proton (i.e. the most energetic particle) must not be compatible with the pion hypothesis;

- when the dE/dx information is available, the difference, normalized to the error, between the measured and the expected values for the candidate proton, must be between -3 and 2 in order to exclude pions;
- the decay particles must have a transverse momentum larger than 20 MeV/c with respect to the V^0 momentum to reject photon conversions to e^+e^- pairs.

The pπ invariant mass spectrum of the V^0 candidates with momentum fraction x_p in the range between 0.25 and 0.5 is shown on figure 6. A clear Λ^0 signal is seen. The average reconstruction efficiency for the detection of a decay $\Lambda \to p\pi$ in this momentum region is estimated from the full DELPHI simulation to be about 7%. The residual K^0_S (decaying into $\pi^+\pi^-$) contamination in the data sample is also studied using the simulation. The effective invariant mass distribution for K^0_S's decays where one pion has been assigned the proton mass is shown shaded in figure 6. Due mainly to the particle identification, the K^0_S contamination is unimportant.

The pπ invariant mass distribution is fitted using a Breit–Wigner function for the signal, the background being described by the formula :

$$B(m) = a \cdot [1 - \exp \frac{-(m-t)}{b}] \tag{9}$$

where a, b and t are free parameters. The fit gives the following results: $m_{\Lambda^0} = 1116.9 \pm 0.4\,(stat.) \pm 0.7\,(syst.)\,\mathrm{MeV}/c^2$ (consistent with the world average of 1115.63 ± 0.05 MeV/c^2 [9]), an average width of about 6.3 MeV/c^2 (for the entire selected momentum range) and a total of $1540 \pm 88\,(stat.) \pm 40\,(syst.)$ Λ^0's were found with a $\chi^2/NDF = 38/30$. The systematic error includes contributions due to the signal and parametrization and changing the mass range used in the fit. The Λ^0 momentum distribution was extracted by fitting the invariant mass distribution of V^0 candidates in several momentum ranges. The resulting experimental Λ^0 distribution is given in figure 7. This distribution has been fitted by an exponential distribution.

In order to compute the asymmetry of the Λ^0 baryons, the following procedure is used. The pπ invariant mass plot in figure 6 is divided into bins of 5 MeV/c^2, and for each bin i the quantity :

$$D_i = N_i^{V^0}(\cos\theta > 0) + N_i^{\overline{V^0}}(\cos\theta < 0) - N_i^{V^0}(\cos\theta < 0) - N_i^{\overline{V^0}}(\cos\theta > 0) \tag{10}$$

is computed, where θ is the angle of the V^0 line-of-flight relative to the incident electron direction. This way, in the absence of biases, the background of fake Λ^0's under the peak is directly subtracted. In each bin of the V^0 mass plot the total number S_i of $\Lambda^0 + \overline{\Lambda^0}$ is obtained by subtracting the fitted contribution of the background :

$$S_i = (N_i^{V,TOT} + N_i^{\bar{V},TOT}) - a\left(1 - \exp\frac{-(m_i - t)}{b}\right). \tag{11}$$

The "signal region" is defined to be the 9 intervals between 1.095 and 1.140 GeV/c^2 in the V^0 mass spectrum where a difference $D = 100 \pm 53(stat.)$ is measured with a total of $S = 1257 \pm 66(stat.)$ $\Lambda^0\overline{\Lambda^0}$ candidates.

The absence of biases has been tested by verifying that:

- the number of Λ^0's is consistent with the number of $\overline{\Lambda^0}$'s (660 ± 49 and 596 ± 50 respectively);
- the number of $\Lambda^0 + \overline{\Lambda^0}$ in the positive hemisphere is consistent with the number of $\Lambda^0 + \overline{\Lambda^0}$ in the negative hemisphere (647 ± 49 and 625 ± 49 respectively);

- no evidence for biases inducing asymmetry signals off the Λ^0 mass peak is found;
- by changing the signal parametrization in the fit, no significant effect is found on S.

In order to account for acceptance effects and angular dependence of the reconstruction efficiency and taking the Λ^0 ($\overline{\Lambda^0}$) direction as an estimator of the direction of the primary quark, the quantity :

$$R(\cos\theta) = \frac{\sum_i D_i(\cos\theta)}{\sum_i S_i(\cos\theta)} \tag{12}$$

is computed in five intervals of $|\cos\theta|$ from 0 to 0.9, where θ is the Λ^0 polar angle and $\sum_i$ the sum over the mass intervals of the "signal region" defined above. The distribution is shown in figure 8. A fit of equation (3) to the distribution gives :

$$A_{FB}^{\Lambda^0} = 0.085 \pm 0.035\ (stat.) \pm 0.018\ (syst.)$$

with $\chi^2/NDF = 1.2/4$.

The error sources contributing to the experimental systematics are listed in table 2. All the contributions to the systematic error are evaluated from the data sample itself. The main contributions come from the definition of the signal region and the Λ^0 selection cuts. The lower x_p limit has been varied by ± 0.01 while the higher limit has been varied asymmetrically by (-0.05, +0.10) to vary equally the number of Λ^0's.

3.3 High energy K_L^0 and neutrons

K_L^0 and neutrons are the only neutral hadrons which can create a hadron shower in the hadron calorimeter. By selecting events with a high energy HCAL shower not associated with any charged particle it is possible to enrich the sample of $s\bar{s}$ and $d\bar{d}$-events. The production of neutrons from initial $u\bar{u}-$states is suppressed due to the isospin suppression of $dd-$diquarks. Due to the energy resolution of the hadron calorimeter, a considerable signal from non-leading neutral particles is also selected. Among these particles, K_L^0 and neutrons from heavy meson decays are selected, giving a contamination from $b\bar{b}$ and $c\bar{c}$ events, while those created in the fragmentation process give a contamination from all quark flavours.

Hadronic events with candidate high momentum neutral hadrons are selected by requiring:

- the deposited energy of the neutral HCAL shower to be larger than 15 GeV;
- the polar angle of the HCAL shower to be between 32° and 148° in order to have well fitted charged tracks in the selected region (at least 40 cm inside the TPC);
- the polar angle of the thrust axis (calculated using only charged particles) to be between 30° and 150°, in order to ensure that the event axis is well contained in the detector;
- the angle between the thrust axis and HCAL shower to be less than 20°;
- the charged energy E_{ch} in each of the hemispheres defined by the plane perpendicular to the thrust axis to be less than 60 GeV (events with E_{ch} greater than 60 GeV include charged particles with unphysical momenta);
- the shower to extend to more than one read-out unit (25 cm iron equivalent) of the hadron calorimeter. This selection is applied in order to remove showers where the length of the shower is too small compared to the expected shower length of a high energy particle.

Finally, if there is more than one neutral HCAL shower in the event, only the most energetic one is considered. Thus, 9565 neutral hadronic shower candidates are retained from the 1992 data. A large fraction (more than 50%) of HCAL showers caused by neutral particles are not found because they are mixed with overlapping showers associated to charged particles. On the other hand, the probability that a charged particle deposing more than 15 GeV in HCAL and satisfying all the previous selection criteria fakes a "neutral" shower is 2.5%. In this way 9% of the selected HCAL showers come from charged particles. For the $s-$ and $d-$quark asymmetry evaluation this effect is taken into account using the full DELPHI simulation.

To tag the primary quark charge, the statistical correlation between the quark charge and the charge flow is used. This technique suggested in [10] has been used at lower energies [11] and recently at LEP experiments [12]. The *sign* of the charge flow Q_{flow} can be used to estimate which hemisphere contains the primary quark. The charge flow is defined as $Q_{flow} = Q_1 - Q_2$, where :

$$Q_1 = \frac{\sum_i q_i |p_{iL}|^\kappa}{\sum_i |p_{iL}|^\kappa} \tag{13}$$

is the momentum-weighted charge in the hemisphere defined by the direction of the neutral HCAL shower and Q_2 is the same variable for the opposite hemisphere. The sum runs over all selected charged particles in each hemisphere, q_i is the measured particle charge and p_{iL} is the momentum component along the vector joining the primary vertex to the HCAL shower. If Q_{flow} is positive (negative), this statistically implies that the neutral HCAL shower is created by a neutral hadron containing the initial positively (negatively) charged quark. According to the simulation, choosing a value of the exponent $\kappa = 0.4$ in equation (13) gives the particle optimal weight in the sum, in order to maximize the correlation between Q_{flow} and the original quark charge.

Figure 9(a) presents the raw differential cross–section of all selected neutral hadrons as a function of $\cos\theta$. Due to the polar angle dependence of the thickness of the penetrated material in front of the hadron calorimeter (1.40 nuclear interaction lengths in the barrel region) and due to the non–uniform detection efficiency of neutral particles, the angular distribution of the neutral hadrons differs from the ideal $1 + \cos^2\theta$ dependence. For this reason a relative weight has been given to each $\cos\theta$ bin to restore the $1+\cos^2\theta$ shape. The correction previously determined has been separately applied to the distribution of neutral hadrons coming from positively and negatively tagged charged primary quarks (according to Q_{flow} value). Figure 9(b) presents the sum of the positively and negatively charged primary quark neutral hadrons as a function of $-sign(Q_{flow}) \cdot \cos\theta$, with $sign(Q_{flow})$ being the sign of Q_{flow}. In order to cross–check the correction corresponding to the detector material, the function $C(1+\cos^2\theta)e^{(-d_0/\sin\theta)}$ has been fitted on the raw neutral hadron distribution (omitting the two central bins). The exponential term describes the material effect which is the dominant one compared to the detector efficiency, while $1 + \cos^2\theta$ describes the ideal distribution. The fitted curve is also shown on figure 9(a). The d_0 parameter has been found to be 1.36 ± 0.05 in agreement with the expected value of 1.40 nuclear interaction lengths. C is a normalization constant left also free in the fit.

By fitting the equation (1) to the $\cos\theta$ distribution shown in figure 9(b), the forward–backward asymmetry of the neutral kaons and neutrons is determined to be :

$$A_{FB}^{(K_L^0,n)} = 0.021 \pm 0.007\ (stat.) \pm 0.012\ (syst.)$$

with a $\chi^2/NDF = 22/26$.

The contributions to the systematic error are listed in table 2. The main contribution comes from the choice of the kinematical variable p_L. The quoted value has been extracted by replacing p_L by the momentum p. The lower energy limit has been varied from 15 to 25 GeV.

4 Calculation of the $s-$quark asymmetry from the measured asymmetries

Two methods, both relying on the JETSET PS model to describe the hadronization process, have been used in the calculation of the s–quark asymmetry from the measured hadron asymmetries. The expected asymmetries for the d and u like flavours (for $\sin^2\theta_W = 0.232$) are 0.100 and 0.071, respectively.

In the first method a global correction function $C^h(x_p)$, calculated from the JETSET simulation program, is applied to the measured asymmetry of each hadron h. This global correction takes into account the dilution of the primary s–quark asymmetry due to some selected hadrons coming from the fragmentation process or from decays of heavier particles generated in the cascade of Z^0 decays into non $s\bar{s}$ final states. The correction function $C^h(x_p)$ is defined by :

$$C^h(x_p) = \frac{A^s_{FB}}{A^h_{FB}(x_p)} \tag{14}$$

where $A^h_{FB}(x_p)$ is the hadron asymmetry for hadrons of momentum fraction x_p calculated using JETSET PS model. The default input value of A^s_{FB} and the DELPHI tuning [7] on JETSET PS parameters have been used. $C^h(x_p)$ has been parametrized as follows :

$$C^h(x_p) = 1 + a^h_0 e^{-a^h_1 x_p} \tag{15}$$

where a^h_0 and a^h_1 are constants specific to each type of hadron.

The mean value in the selected momentum range of each hadron has to be calculated. The distribution $f^h(x_p) = b^h_0 \cdot e^{-b^h_1 x_p}$ describes well the reconstructed hadron momentum distribution (figures 4 and 7). The overall asymmetry correction factor α^h is defined to be :

$$\alpha^h = \frac{\int_{x_p^{min}}^{x_p^{max}} f^h(x_p) C^h(x_p) dx_p}{\int_{x_p^{min}}^{x_p^{max}} f^h(x_p) dx_p} \tag{16}$$

where x_p^{min} and x_p^{max} are the limits of the hadron selected momentum interval. Finally, the measured $s\bar{s}$ asymmetry is :

$$A^s_{FB} = \alpha^h \cdot A^h_{FB} \; . \tag{17}$$

Table 3 gives the values of the quantities a^h_0, a^h_1 and b^h_1 (b^h_1 is the raw measured value) defined above while figure 10 presents the variation of C^h as a function of x_p for $K^\pm$ and Λ^0. The global correction method has not been applied to the neutral hadron sample due to the poor energy resolution of the hadron calorimeter.

In the second method, the measured asymmetry for each hadron type is assumed to be a statistical average of all quark flavour asymmetries weighted by a factor estimated from simulation. This factor depends on the fractions of the selected hadrons produced in each flavour event and on the probability of tagging the primary quark charge correctly.

In this way, the measured asymmetry can be expressed as :

$$A^h_{FB}(meas.) = \sum_f \alpha^h_f (2\epsilon^h_f - 1) A^f_{FB} \tag{18}$$

where α^h_f is the fraction of hadrons produced in events of flavour f and ϵ^h_f is the probability of tagging the primary quark charge in the same hemisphere correctly. The q–quark asymmetry can be expressed by :

$$A^q_{FB} = \frac{A^h_{FB}(meas.) - \sum_{f \neq q} \alpha^h_f (2\epsilon^h_f - 1) A^f_{FB}}{\alpha^h_q (2\epsilon^h_q - 1)} \tag{19}$$

where $q = s$ for the charged kaon and Λ^0 measurements and $q = s, d$ for neutral hadrons. Table 4 gives the values of α^h_f, ϵ^h_f for the three hadron species used.

Results on A^s_{FB} are affected by statistical and systematic errors. The statistical error on A^s_{FB} is obtained by propagating the statistical error on $A^h_{FB}(meas.)$ according to the correction method. The measured values for the three hadron species are :

$$A^s_{FB}(K^\pm) = \begin{cases} 0.118 \pm 0.027\ (stat.) \pm 0.015\ (syst.) & \text{global method} \\ 0.128 \pm 0.037\ (stat.) \pm 0.013\ (syst.) & \text{weighted method} \end{cases}$$

$$A^s_{FB}(\Lambda^0) = \begin{cases} 0.134 \pm 0.055\ (stat.) \pm 0.037\ (syst.) & \text{global method} \\ 0.164 \pm 0.109\ (stat.) \pm 0.057\ (syst.) & \text{weighted method} \end{cases}$$

$$A^{s,d}_{FB}(K^0_L, n) = 0.112 \pm 0.031\ (stat.) \pm 0.054\ (syst.) \text{ weighted method.}$$

For the weighted method the measured asymmetry values of equation (6) have been used [1] with the following assumptions :

- the central values for A^d_{FB} and A^u_{FB} are equal to the measured values of A^b_{FB} and A^c_{FB}, respectively;
- $A^d_{FB} = A^s_{FB}$ for the neutral hadron measurement;
- the errors on A^d_{FB} and A^u_{FB} are 3 times larger than the corresponding measured errors on A^b_{FB} and A^c_{FB} (used for systematic error evaluation).

Contributions due to the limited number of simulated events (20 million JETSET PS events) are included in the systematic error. Different contributions must be taken into account to evaluate the total systematic error on A^s_{FB}. Some of them are common to both correction methods applied to the different data samples. All contributions are given in tables 5 and 6 and listed below:

- experimental method (details are given in table 2);
- uncertainties on the parameters used in the correction methods (correction factor for the global method and α^h_f, ϵ^h_f for the weighted method);
- uncertainties on measured values A^c_{FB} and A^b_{FB}.
- parametrization of the fragmentation process and uncertainties on the decay branching fractions at the generator level.

An error coming from the fact that the hadron direction is used for the asymmetry evaluation instead of the primary quark direction (which is unknown) is already included in the correction factors of the two methods. No difference is observed between the asymmetry obtained using the hadron direction and the one obtained using the thrust axis of the event. Using the simulation no significant difference is expected between the

distributions of the angle between the primary quark direction and the thrust axis and the angle between the primary quark direction and the hadron direction.

For the global correction method, the contribution of the parametrization function for the dN/dx_p distribution must be added. The systematic contributions to the error on A^s_{FB} using this method for the fast charged kaon and the fast Λ^0 samples are listed in table 5.

The systematic contributions to the error on A^s_{FB} calculated with the weighted method are listed in table 6. For charged kaons and Λ^0's the parameters α^h_f and ϵ^h_f have been convoluted with the experimental dN/dx_p distribution and include a systematic uncertainty. For neutral hadrons, the DELSIM simulation program has been used to extract these two parameters.

A detailed study of the uncertainties due to the hadronization model (JETSET PS) parameters has been performed. Results were obtained by generating 20 million events for each parameter value applying the momentum and angular acceptance selections. The list of the parameters tested is presented in table 7 with their reference values. Table 7 gives also the limits between which these parameters have been varied and the corresponding variations of the asymmetry. These variations have been calculated using the weighted method. They are not included in the errors of the weighted method parameters α^h_f and ϵ^h_f quoted in table 4 which include only the errors coming from the limited statistics of simulated events and the dN/dx_p parametrization. Also listed in table 7 are the contributions to the systematic error on A^s_{FB} obtained from the fast Λ^0 sample due to the uncertainties on the branching ratios of inclusive decays of Λ_c and B mesons into Λ^0. Some other parameters ($\Gamma_{c\bar{c}}/\Gamma_{had}$, $\Gamma_{b\bar{b}}/\Gamma_{had}$, $B \to \Lambda^0 + X$ branching ratio ...) have also been varied but their contribution has been found to be negligible compared to the reported contributions.

The dominant error coming from fragmentation for charged kaons comes from the variation of γ_s/γ_u (suppression of $s-$quark pair production) [13] while for Λ^0's the dominant error comes from "popcorn" mechanism parameter [14]. For neutral hadrons the main contributions come from the Peterson parameter ϵ_c [7] and from the cut–off value Q_0 of parton shower evolution.

Finally, the main systematic error for charged kaons comes from the uncertainty on the correction factor for the global method and from the hadronization description in simulation for the weighted method. For Λ^0's and neutral hadrons the main contribution for both methods comes from the experimental method. The total systematic contributions are summarized in the next section where the final results and errors for the quantity A^s_{FB} are quoted.

5 Results

Combining the two measurements of A^s_{FB} (using $K^\pm$ and Λ^0's) for each method separately, the $s-$quark forward–backward asymmetry is obtained :

$$\begin{aligned} A^s_{FB}(global) &= 0.121 \pm 0.024\ (stat.) \pm 0.014\ (syst.) \\ A^s_{FB}(weighted) &= 0.131 \pm 0.035\ (stat.) \pm 0.013\ (syst.)\ . \end{aligned}$$

The two results are consistent within the errors but they have different physical significance. In the global correction method all relations between quark asymmetries and electroweak parameters are fixed by the Standard Model predictions. The correction factor α^h of the global method depends only slightly on the effective leptonic $\sin^2\theta^{eff}_W$

(variation of α^h less than 1% for a 3σ variation of $\sin^2\theta_W^{eff}$ around the LEP average [1]) and the asymmetry measured using this method can be used to calculate $\sin^2\theta_W^{eff}$ (with large errors compared to the $b-$quark asymmetry measurement). In order to extract from the measured asymmetry the $\sin^2\theta_W^{eff}$ using equations (4) and (5), the corrections suggested in [1] have been applied taking into account the difference between the $b-$quark and $s-$quark case mainly for QCD corrections. The following value is obtained :

$$\sin^2\theta_W^{eff} = 0.2273 \pm 0.0043\ (stat.) \pm 0.0025\ (syst.).$$

No significant difference is observed between this value and the LEP average [1] extracted using $b-$quark events (0.2327 ± 0.0007).

The weighted method, making only the assumption that the u and d asymmetries are the same as the measured c and $b-$quark asymmetries, respectively, is less Standard Model dependent and can be considered as a universality check of the coupling constant. No significant difference is observed between the weighted method asymmetry and the $b-$quark asymmetry quoted in Ref. [1] (see equation 6).

6 Conclusion

The forward–backward asymmetries of fast $K^{\pm}$, Λ^0's and K_L^0+n have been measured at the Z^0 peak. From these measurements two different methods have been used to extract the $s-$quark asymmetry. Systematic errors on this measurement have been determined using JETSET 7.3 PS model. The result from the two methods are :

$$\begin{aligned} A_{FB}^s(global) &= 0.121 \pm 0.024\ (stat.) \pm 0.014\ (syst.) \\ A_{FB}^s(weighted) &= 0.131 \pm 0.035\ (stat.) \pm 0.013\ (syst.)\ . \end{aligned}$$

in agreement with each other.

These result can be compared with the $b-$quark asymmetry $A_{FB}^b = 0.0915 \pm 0.0037$ (from LEP experiments) to test the universality of the coupling constants. No significant difference is observed between the two measurements.

From the neutral hadron method the following value for the unresolved d and s asymmetry is obtained :

$$A_{FB}^{s,d} = 0.112 \pm 0.031\ (stat.) \pm 0.054\ (syst.)$$

which is compatible with the previous values.

Acknowledgements

We are greatly indebted to our technical collaborators and to the funding agencies for their support in building and operating the DELPHI detector, and to the members of the CERN-SL Division for the excellent performance of the LEP collider.

References

[1] The LEP Collaborations and the LEP Electroweak Working Group, "Combined Preliminary Data on Z^0 Parameters from the LEP Experiments and Constraints on the Standard Model", CERN-PPE/94-187 (1994).

[2] T. Sjöstrand, Comp. Phys. Comm. **27** (1982) 243; ibid. **28** (1983) 229;
T. Sjöstrand, "PYTHIA 5.6 and JETSET 7.3", CERN-TH.6488/92 (1992).

[3] P. Aarnio et al. (DELPHI collab.), Nucl. Instr. and Meth. **A303** (1991) 233.

[4] P. Aarnio et al. (DELPHI collab.), Phys. Lett. **B240** (1990) 271.

[5] E.G. Anassontzis et al., Nucl. Instr. and Meth. **A323** (1992) 351.

[6] DELSIM User's Guide, DELPHI Note 89-15 PROG 130, CERN, February 1989;
DELSIM Reference Manual, DELPHI Note 89-68 PROG 143, CERN, September 1989.

[7] W. de Boer et al., IEKP-KA/91-07, Karlsruhe, June 1991;
T.Todorov, PhD Thesis, Université Louis Pasteur Strasbourg, CRN/HE 94–21 (1994).

[8] For RICH error calculations see for example:
T. Ekelöf, "The Experimental Method of Ring–Imaging Cherenkov (RICH) Counters", CERN EP 84–168 (1984);
T. Ypsilantis, "Particle Identification at Hadron Colliders", in ECFA Study Week, E. Fernandez and G. Jarlskog Eds, CERN 89-10 (1989) 661;
J. Seguinot and T. Ypsilantis, "Ring Imaging Cherenkov Counters", CERN–LAA/PI/91–004 (1991).

[9] Particle Data Group, "Review of Particle Properties", Phys. Rev. **D50**, Part I (1994).

[10] R. Field and R. Feynman, Nucl. Phys. **B136** (1978) 1.

[11] W.W. Ash et al. (MAC Collab.), Phys. Rev. Lett. **58** (1987) 1080;
T. Greenshaw et al. (JADE Collab.), Zeit. Phys. **C42** (1989) 1.

[12] D. Decamp et al. (ALEPH Collab.), Phys. Lett. **B259** (1991) 337;
P. Abreu et al. (DELPHI Collab.), Phys. Lett. **B277** (1992) 371;
P.D. Acton et al. (OPAL Collab.), Phys. Lett. **B294** (1992) 436.

[13] P. Abreu et al. (DELPHI Collab.), Phys. Lett. **B275** (1992) 231.

[14] P. Abreu et al. (DELPHI Collab.), Phys. Lett. **B318** (1993) 249.

Table 1: Expected asymmetry and fraction for charged kaons ($10 < p_K < 18$ GeV/c), Λ^0's ($11.41 < p_{\Lambda^0} < 22.82$ GeV/c) and neutral hadrons (energy greater than 15 GeV) for each quark flavour from JETSET PS model.

Flavour	K^-		Λ^0		$(\overline{K^0_L}, n)$	
	asymmetry	fraction	asymmetry	fraction	asymmetry	fraction
d	-0.035	11.5 %	+0.044	13.7 %	+0.032	24.0 %
u	-0.032	10.3 %	+0.037	10.5 %	-0.037	9.6 %
s	+0.069	43.0 %	+0.089	42.6 %	+0.034	44.8 %
c	+0.047	22.1 %	+0.064	17.7 %	-0.036	12.6 %
b	+0.062	13.1 %	+0.080	15.5 %	+0.032	9.0 %
total	+0.041	100 %	+0.072	100 %	+0.018	100 %

Table 2: Contributions to the systematic error on measured hadron asymmetry A^h_{FB} due to the experimental method.

Systematic error	$\Delta A^{K^\pm}_{FB}$	$\Delta A^{\Lambda^0}_{FB}$	$\Delta A^{(K^0_L,n)}_{FB}$
Different interaction with materials	± 0.0005	–	–
Variation of the momentum or energy range	± 0.0005	± 0.005	± 0.006
Signal parametrization	± 0.0020	± 0.004	–
Definition of signal width region	–	± 0.012	–
Selection cuts	–	± 0.012	–
Choice of the kinematical variable in Q_{flow}	–	–	± 0.010
Parameter κ in Q_{flow} (0.3–0.5)	–	–	± 0.004
Total systematic error	± 0.0021	± 0.018	± 0.012

Table 3: Correction factors for $K^\pm$ and Λ^0 used in global method (b^h_1 is the slope of the exponential distribution fitted to the experimental momentum distribution).

factor	$K^\pm$	Λ^0
a^h_0	2.81 ± 0.35	3.18 ± 1.01
a^h_1	2.32 ± 0.40	5.54 ± 0.81
b^h_1	8.86 ± 0.56	13.16 ± 0.76
α^h	2.46 ± 0.25	1.58 ± 0.23

Table 4: Fraction α_f^h of hadrons produced and tagging probability ϵ_f^h of the quark direction for each flavour f according to the simulation. The quantities α_f^h and ϵ_f^h have been weighted according to the experimental momentum distributions.

f	$K^\pm$		Λ^0		(K_L^0, n)	
	α_f^h	ϵ_f^h	α_f^h	ϵ_f^h	α_f^h	ϵ_f^h
d	0.1151 ± 0.0008	0.3229 ± 0.0012	0.1446 ± 0.0023	0.719 ± 0.015	0.240 ± 0.006	0.662 ± 0.015
u	0.1031 ± 0.0008	0.2775 ± 0.0011	0.1112 ± 0.0018	0.732 ± 0.022	0.096 ± 0.004	0.240 ± 0.021
s	0.4279 ± 0.0014	0.8430 ± 0.0010	0.3901 ± 0.0076	0.913 ± 0.013	0.448 ± 0.008	0.672 ± 0.011
c	0.2220 ± 0.0008	0.8300 ± 0.0011	0.1803 ± 0.0031	0.910 ± 0.022	0.126 ± 0.005	0.245 ± 0.018
b	0.1319 ± 0.0011	0.8082 ± 0.0008	0.1739 ± 0.0026	0.903 ± 0.017	0.090 ± 0.004	0.662 ± 0.024

Table 5: Contributions to the systematic error on A_{FB}^s for the global correction method. The error quoted for the correction factor includes limited amount of simulated events and dN/dx_p parametrization.

systematic error source (global correction method)	$\Delta A_{FB}^s(K^\pm)$	$\Delta A_{FB}^s(\Lambda^0)$
Experimental method	± 0.005	± 0.030
Correction factor	± 0.012	± 0.020
Hadronization description in simulation	± 0.008	± 0.006
Total	± 0.015	± 0.037

Table 6: Contributions to the systematic error on A_{FB}^s for the weighted method. The errors quoted for α_f^h and ϵ_f^h include limited amount of simulated events and dN/dx_p parametrization for $K^\pm$ and Λ^0.

systematic error source (weighted method)	$\Delta A_{FB}^s(K^\pm)$	$\Delta A_{FB}^s(\Lambda^0)$	$\Delta A_{FB}^{d,s}(K_L^0, n)$
Experimental method	± 0.0072	± 0.056	± 0.052
α_f^h	± 0.0005	± 0.003	± 0.002
ϵ_f^h	± 0.0004	± 0.006	± 0.007
Experimental values of $A_{FB}^{f \neq s(,d)}$	± 0.0065	± 0.007	± 0.007
Hadronization description in simulation	± 0.0080	± 0.006	$^{+0.016}_{-0.004}$
Total	± 0.0126	± 0.057	± 0.054

Table 7: Systematic errors on A_{FB}^f (calculated using the values of table 4) resulting from JETSET PS parameters. Λ_{QCD}, ϵ_c and ϵ_b have been varied independently. For 11 and 13 the variations are related to the JETSET 7.3 PS values.

Num.	Parameter	Reference value	Variation tested	ΔA_{FB}^s $(K^{\pm})$	ΔA_{FB}^s (Λ^0)	ΔA_{FB}^{sd} (K_L^0, n)
1	Λ_{QCD}	315 MeV	$^{230}_{400}$ MeV	∓ 0.001	∓ 0.001	$^{+0.003}_{+0.006}$
2	Cut-off value Q_0 of parton shower evolution	1 GeV	$^{0.6}_{1.4}$ GeV	∓ 0.002	–	$^{+0.007}_{+0.005}$
3	Width σ_{p_T} of Gaussian p_T distribution	395 MeV	$^{365}_{425}$ MeV	∓ 0.001	–	$^{+0.004}_{+0.005}$
4	Parameter a of Lund symmetric fragmentation function	0.20	$^{0.14}_{0.26}$	± 0.001	± 0.001	$^{-0.001}_{+0.004}$
5	Parameter ϵ_c of Peterson fragmentation function	-0.054	$^{-0.030}_{-0.071}$	∓ 0.004	∓ 0.003	$^{+0.009}_{-0.003}$
6	Parameter ϵ_b of Peterson fragmentation function	-0.006	$^{-0.003}_{-0.010}$	∓ 0.001	∓ 0.001	$^{-0.001}_{+0.005}$
7	Suppression of $s-$quark pair production γ_s/γ_u	0.30	$^{0.28}_{0.32}$	∓ 0.005	∓ 0.002	$^{-0.002}_{+0.002}$
8	Probability to generate a prompt spin 1 meson $V/(V+PS)$	0.70	$^{0.52}_{0.88}$	± 0.002	± 0.001	$^{-0.001}_{+0.003}$
9	Suppression of strange diquark production $(\gamma_{us}/\gamma_{ud})/(\gamma_s/\gamma_d)$	0.34	$^{0.27}_{0.41}$	–	± 0.002	$^{+0.001}_{+0.002}$
10	"Popcorn" mechanism for Λ^0 production	0.70	$^{0.50}_{0.90}$	–	± 0.004	–
11	$Br(\Lambda_c \to \Lambda^0 + anything)$	27%	$^{+2\times}_{-0.5\times}$	–	± 0.001	–
12	$B - \overline{B^0}$ mixing parameter (x_d)	0.70	$^{0.90}_{0.50}$	± 0.002	∓ 0.001	–
13	$Br(D^0 \to K^+/K^- + anything)$ $Br(D^+ \to K^+/K^- + anything)$ $Br(D_s^+ \to K^+/K^- + anything)$	3.4%/46% 5.8%/20.8% 20%/13%	$\pm 0.10\times$ $\pm 0.15\times$ $\pm 0.90\times$	± 0.001	–	–
$\Delta A_{FB}^s(total)$				± 0.008	± 0.006	$^{+0.016}_{-0.004}$

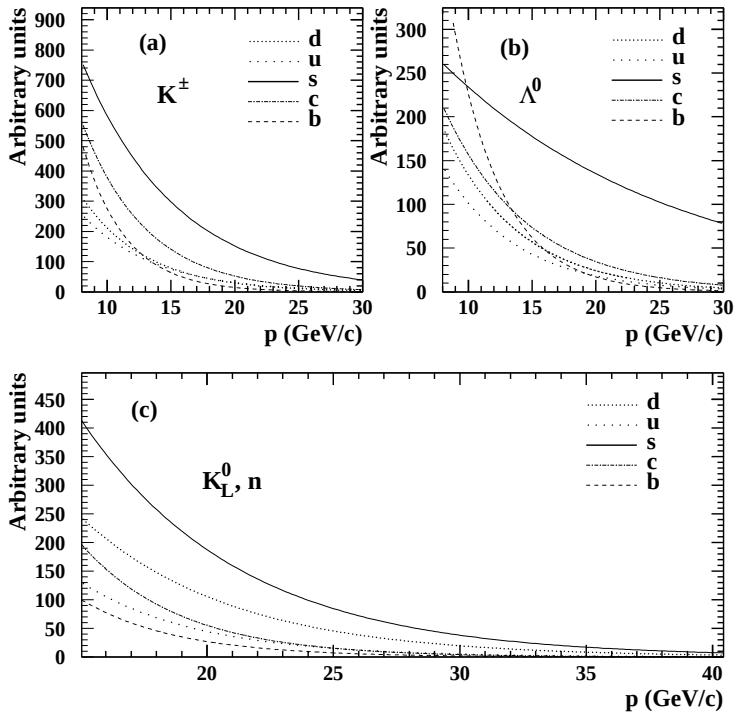

Figure 1: (a) $K^{\pm}$ (b) Λ^0 and (c) K^0_L, n momentum distribution separately for the five quark flavours in the JETSET 7.3 PS model.

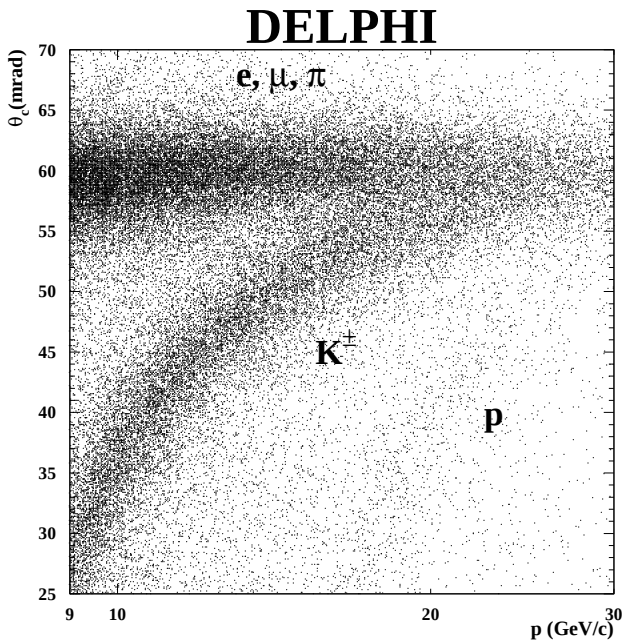

Figure 2: Mean Cherenkov angle versus particle momentum.

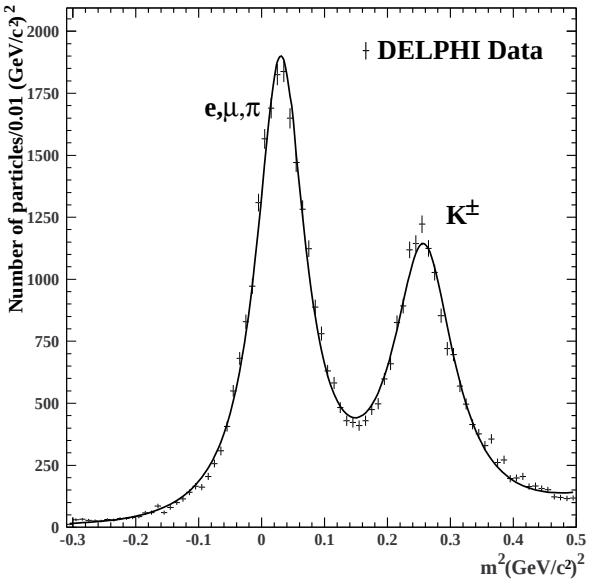

Figure 3: Mass squared distribution using the RICH detector for all charged particles with $10 < p < 18$ GeV/c. The curve shows the fit of two Breit–Wigner distributions.

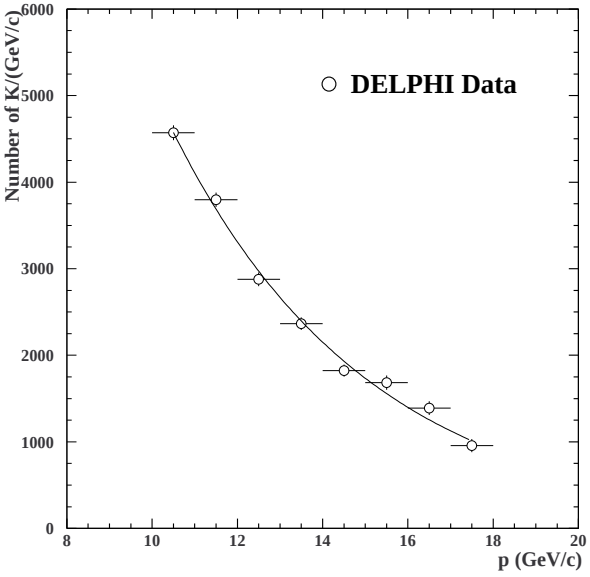

Figure 4: Raw charged kaon momentum distribution extracted using RICH information. The curve represents the fit of an exponential distribution.

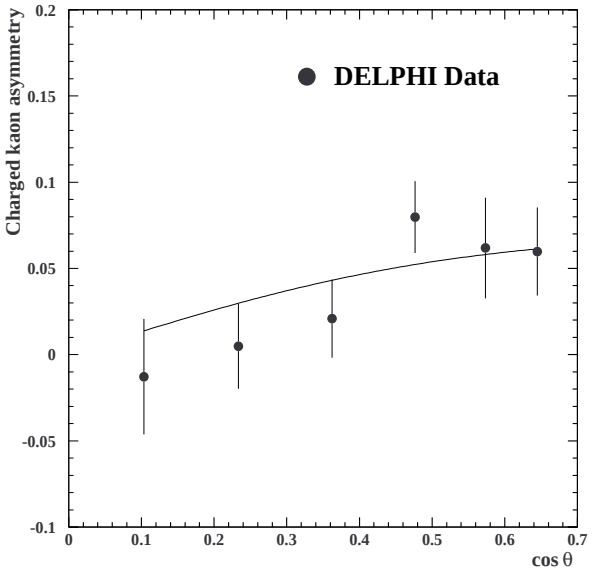

Figure 5: Charged kaon asymmetry as a function of the cosine of the polar angle θ. Equation (3) has been fitted to these data (curve).

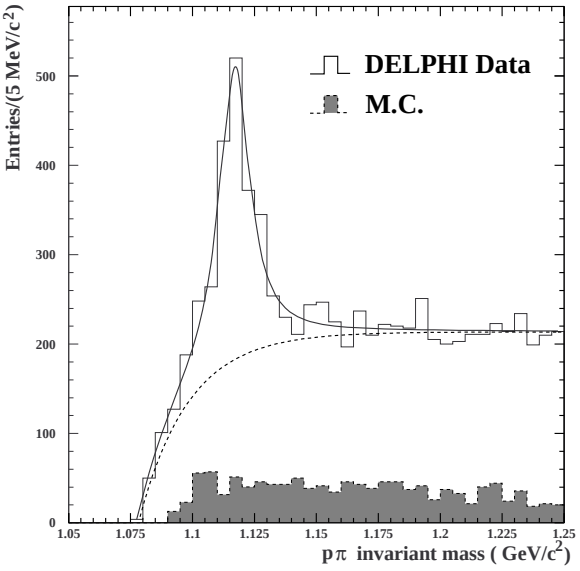

Figure 6: pπ invariant mass spectrum for $0.25 < x_p < 0.5$ (solid line histogram). The solid curve represents the signal plus background parametrization while the dashed curve shows only the background contribution. The expected K^0_S (decaying into $\pi^+\pi^-$) reflection is also shown (grey area).

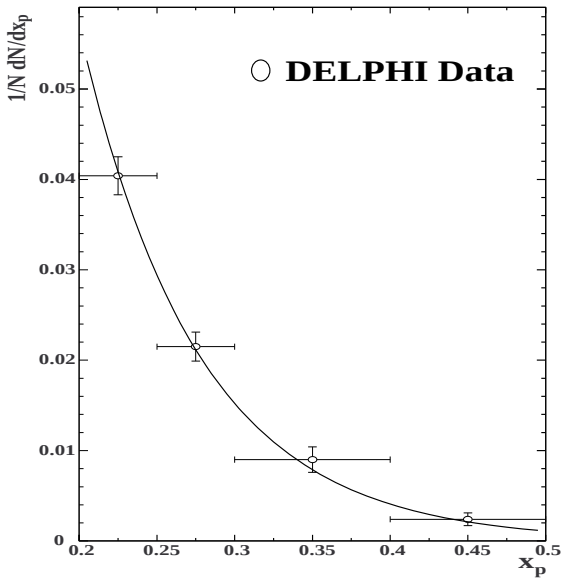

Figure 7: Experimental Λ^0 x_p distribution. The curve represents the fit of an exponential distribution.

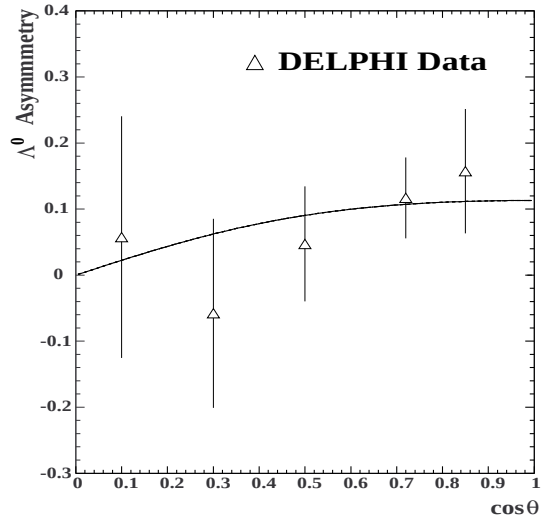

Figure 8: Λ^0 asymmetry as a function of the cosine of the polar angle θ. Equation (3) has been fitted to these data (curve).

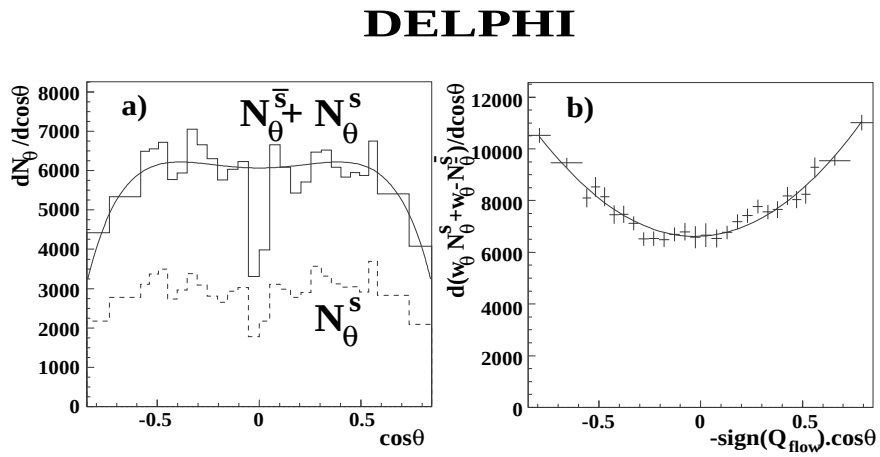

Figure 9: (a) Raw distribution of $\cos\theta$ for all selected neutral hadrons ($K_L^0,\ n$) detected as hadron calorimeter showers (b) Sum of the neutral hadrons coming from positively ($N_\theta^{\bar{s}}$) and negatively (N_θ^s) charged tagged partons after taking into account the detector efficiency and the material effect. The curves are described in the text.

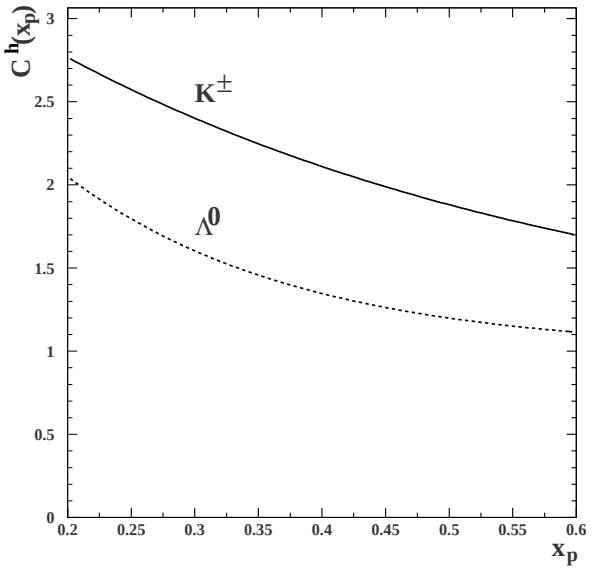

Figure 10: Correction factor of global method for $K^\pm$ (continuous curve) and Λ^0 (dashed curve).